

## Study of structural-, compositional-, and thickness-dependent thermoelectric and electrical properties of Bi<sub>93</sub>Sb<sub>7</sub> alloy thin films

Ramesh Chandra Mallik and V. Damodara Das

Citation: *Journal of Applied Physics* **98**, 023710 (2005); doi: 10.1063/1.1957126

View online: <http://dx.doi.org/10.1063/1.1957126>

View Table of Contents: <http://scitation.aip.org/content/aip/journal/jap/98/2?ver=pdfcov>

Published by the [AIP Publishing](#)

---

### Articles you may be interested in

[Thickness dependence oscillations of transport properties in thin films of a topological insulator Bi<sub>91</sub>Sb<sub>9</sub>](#)  
*Appl. Phys. Lett.* **101**, 023108 (2012); 10.1063/1.4730950

[Electric current enhanced defect elimination in thermally annealed Bi–Sb–Te and Bi–Se–Te thermoelectric thin films](#)  
*J. Appl. Phys.* **108**, 053711 (2010); 10.1063/1.3477184

[Thermoelectric properties of electrically stressed Sb/Bi–Sb–Te multilayered films](#)  
*J. Appl. Phys.* **107**, 066103 (2010); 10.1063/1.3326878

[Enhancement of thermoelectric properties of sputtered Bi–Sb–Te thin films by electric current stressing](#)  
*Appl. Phys. Lett.* **93**, 042103 (2008); 10.1063/1.2965487

[Thermoelectric transport properties of n-doped and p-doped Bi<sub>0.91</sub>Sb<sub>0.09</sub> alloy thin films](#)  
*J. Appl. Phys.* **85**, 3655 (1999); 10.1063/1.369729

---



# Study of structural-, compositional-, and thickness-dependent thermoelectric and electrical properties of $\text{Bi}_{93}\text{Sb}_7$ alloy thin films

Ramesh Chandra Mallik and V. Damodara Das<sup>a)</sup>

*Thin Film Laboratory, Department of Physics, Indian Institute of Technology, Madras, Chennai 600 036, India*

(Received 24 January 2005; accepted 27 May 2005; published online 26 July 2005)

We have used the melt-quenching technique to prepare the bulk material and vapor-quenching technique to prepare the thin films of  $\text{Bi}_{93}\text{Sb}_7$  alloy. The  $\text{Bi}_{93}\text{Sb}_7$  alloy thin films of different thicknesses were grown onto well-cleaned glass and silicon substrates. The films were annealed at  $150^\circ\text{C}$  for 4 h in a vacuum of the order of  $10^{-6}$  torr in order to remove the defects and to increase the grain size. The bulk and thin-film x-ray diffraction results agree with the transmission electron microscopy results and the compositional analysis of bulk by particle-induced x-ray emission and of thin films by Rutherford backscattering. The thickness and temperature dependences of thermoelectric power and electrical resistivity have been analyzed. The negative temperature coefficient of resistivity confirmed that the material is semiconducting in nature. The negative thermoelectric power confirmed that the present bismuth-rich material is a  $n$  type. In this paper we have made an attempt to study the thermoelectric properties of bulk as well as thin films of  $\text{Bi}_{93}\text{Sb}_7$ , maintaining the same composition. The scattering index parameter was calculated from the experimental data and was compared with the theoretical predictions of the size effect theory. © 2005 American Institute of Physics. [DOI: 10.1063/1.1957126]

## I. INTRODUCTION

The Bi–Sb alloys have attracted thermoelectric researchers due to their high thermoelectric power, high mobility, and small thermal conductivity. This narrow-band-gap semiconductor  $\text{Bi}_{1-x}\text{Sb}_x$  ( $0.04 < x < 0.22$ ) is thermoelectrically important material in the above composition range and is used in thermoelectric coolers and sensors. This material is a semimetal, which belongs to the fifth group of the periodic table with the rhombohedral (SG:  $R-3m$ ) structure. When bismuth combines with antimony to form a Bi–Sb alloy over wide ranges of composition, the crystal structure and concentration of electrons and holes remain the same but the band structure continuously changes. The details of band structures were discussed by Mustafaev.<sup>1</sup> Both bismuth and antimony have five valence electrons per atom. Atoms combine themselves in a pair-pair crystal lattice giving two ions and ten electrons per unit cell. It is slightly distorted from the cubic lattice and this small distortion from the cubic lattice gives rise to overlapping of bands. So, bismuth and antimony are semimetals in nature where fifth and sixth bands overlap and contribute lesser number of electrons and holes at all temperatures.<sup>2</sup>

In the alloys of bismuth and antimony ( $\text{Bi}_{1-x}\text{Sb}_x$ ) (Ref. 3) in the composition range ( $0.04 < x < 0.22$ ) there is a band gap of the order of 20–38 meV and the alloy is semiconducting in nature. Beyond this composition range, it is semimetallic. Jain<sup>4</sup> has shown that when Sb concentration reaches about 5%, the alloy becomes semiconducting and the forbidden energy gap increases to a peak at about 12% of Sb. Lenoir *et al.*<sup>3</sup> have shown that the energy gap is nearly 38 meV when  $x=0.15$ .

The efficiency of a thermoelectric material is given by a quantity called the figure of merit, defined as  $Z=S^2\sigma/K$ , where  $S$  is the thermoelectric power,  $\sigma$  is the electrical conductivity, and  $K$  is the thermal conductivity. The figure of merit  $Z$  depends on the scattering mechanism operating in the thin films due to several factors such as scattering from impurity atoms/ions, lattice, and grain boundaries. The electronic and transport properties of the present material are very sensitive towards the impurities especially at low temperatures. The  $n$ -type and  $p$ -type impurity-doped  $\text{Bi}_{91}\text{Sb}_9$  and artificially ordered bismuth and antimony superlattice alloys have been studied by Cho *et al.*<sup>5,6</sup> In this paper we have discussed the nature of scattering in thin films of  $\text{Bi}_{93}\text{Sb}_7$ , grown by vacuum flash evaporation technique, which directly affects the thermoelectric properties. Particle-induced x-ray emission (PIXE) and Rutherford backscattering (RBS) analyses have been used to determine the composition of the constituent materials present in the bulk as well as the as-grown and annealed films of different thicknesses.

## II. EXPERIMENTS

The melt-quench technique was used for the preparation of the bulk sample of  $\text{Bi}_{93}\text{Sb}_7$  alloy. The two elements in the required ratio of atomic weights of bismuth and antimony were taken in the quartz tube, and, it was evacuated to a high vacuum of the order of  $10^{-5}$  torr. The quartz tube was sealed and then heated in an electric furnace. The temperature of the furnace was set at  $750^\circ\text{C}$  according to the phase diagram.<sup>7</sup> The bulk sample was quenched to liquid-nitrogen temperature from  $750^\circ\text{C}$  because it was seen from the phase diagram that there is a wide gap between the solid state and the liquid state. For the confirmation of the single phase, x-ray diffraction (XRD) analysis was carried out in the machine Shimad

<sup>a)</sup>Electronic mail: vddas@iitm.ac.in

2V of model XD-D1 using the radiation  $\text{Cu } K\alpha 1$  with a wavelength of 1.5418 Å. To avoid the dissociation or decomposition of the material, the thin films of  $\text{Bi}_{93}\text{Sb}_7$  alloys were grown by the flash evaporation vapor-quenching technique on both glass and silicon wafer substrates in a single deposition in the vacuum of  $10^{-5}$  torr. The vapors of the above materials rapidly fall from a very high temperature to room temperature and the thin films are formed. So, there will be very little possibility of dissociation or decomposition of the material. The films were annealed at 423 K for 4 h in the vacuum chamber at a pressure of  $10^{-6}$  torr. For RBS study, the films grown on silicon wafers were used and the films grown on the glass substrates were used for transmission electron microscopy (TEM) and XRD studies. The TEM study was carried out in Philips CM-12 model electron microscope. The magnification of the micrograph was 35 000 x, the beam current was 10  $\mu\text{A}$ , the accelerating voltage of the electrons was 120 KV, and the camera length for the selected area electron diffraction (SAED) pattern was 770 mm. The RBS studies were done to know the composition of the formed films and for their thickness measurement.

The low-impurity concentration detection in thin films, by the RBS technique, has been discussed by several authors.<sup>8-12</sup> The experimental details of the RBS technique are given elsewhere.<sup>13-15</sup> The RBS experiment was carried out using the Tandem Pelletron Accelerator facility available at the Ion Beam Laboratory at the Institute of Physics, Bhubaneswar, India. The films of  $\text{Bi}_{93}\text{Sb}_7$  deposited onto silicon substrates were used for the RBS study. The main aim for the selection of the substrate for RBS study was that the substrate should be conducting to avoid the surface charge accumulation, as silicon is a conducting substrate and also has a low atomic number of 14, which is much lower compared with the atomic numbers of bismuth and antimony. Due to the low atomic number of the substrate and the high atomic number of the thin films, the RBS spectra can be well distinguished. Hence, silicon substrates are more suitable than any other substrates. There are several authors who have described Rutherford backscattering in a thin crystalline lattice.<sup>16-18</sup> The high-energy  $\text{He}^{++}$  beam of  $\sim 3.05\text{-MeV}$  energy and a current of  $\sim 15$  nA was made to be incident normal to the surface of the film. The surface-barrier detector was kept at an angle of  $165^\circ$  to the incident beam. Data acquisition was done using a computer in the case of both as-grown and annealed films. The energy resolution was 15 keV and the ion current was 15 nA. In order to analyze the backscattering spectrum, we have used the computer program of GISA3 to simulate the spectrum. The particle-induced x-ray emission analysis was done to determine the atomic concentration of the constituent elements. PIXE measurements were carried out using the Tandem Pelletron Accelerator facility available at IOP, Bhubaneswar, India. Samples were made in the form of pellets from the finely powdered ingots. Since the measurements under vacuum demand conducting specimens, graphite was used as a binding material. Fine powder of  $\text{Bi}_{93}\text{Sb}_7$  was mixed with highpurity graphite powder in the ratio of 1:1 by weight. After thorough mixing, pellets were obtained by pressing in a hydraulic press. In order to identify the relative peak positions of x-ray emission

lines of constituent elements, PIXE spectra of the elements, namely, bismuth and antimony were also taken.  $\text{Bi}_{93}\text{Sb}_7$  along with bismuth and antimony pellet standards were fixed on the sample holder and then loaded onto the PIXE chamber. The chamber was evacuated to a pressure of  $\sim 10^{-6}$  torr. Collimated proton beam of 3-MeV energy was used to irradiate the samples. Measurements were made with a maximum beam current of  $\sim 6$  nA. Liquid-nitrogen-cooled energy dispersive Si(Li) detector (Canberra, active area of 30  $\text{mm}^2$ , beryllium window) having a resolution of 170 eV at 5.9 keV was used. The detector was kept at  $90^\circ$  to the incident beam. Characteristic x rays emitted from the samples exit the PIXE chamber through a 50- $\mu\text{m}$  mylar window before entering the detector. Spectra were recorded using a Canberra series S-100 multichannel analyzer (MCA).

Out of several methods, we have used the integral method for the thermoelectric power measurement in the temperature range of 100–300 K using high accuracy Keithley digital multimeters. The cold-finger-type cryostat was used for the measurement of thermoelectric power at a high vacuum of  $\sim 10^{-6}$  mbar. The total measurement process was fully automated and controlled using the IEEE interfacing card with the computer. For each time interval of 20 s, the data were acquired. The system was calibrated using a copper/constantan film thermocouple. The contacts were made using high-purity copper wire so that the absolute thermoelectric power can be obtained by subtracting the copper thermoelectric power. For thermoelectric power measurements, the sample size was  $1 \times 7$   $\text{cm}^2$  and as we need the thermal gradient, we had to keep one end of the sample at a low temperature and the other end at room temperature which was maintained by a small 40-W heater.

Out of several methods, we make use of the conventional van der Pauw<sup>19</sup> method for the electrical resistivity measurement. In the resistivity measurement one should avoid the thermal voltage produced by  $\Delta T$ , and for that one should change the direction of current through the sample and take the average of the voltages. But to get more accurate results, the sample should be placed in such a way that there is no thermal gradient across the sample. In our resistivity measurements we have used the sample size of  $1 \times 1$   $\text{cm}^2$  and the sample was kept horizontally in the sample holder in the cryostat. The resistivity and thermoelectric power measurements were made on samples of different thicknesses between 100 and 300 K. The accuracy of voltage measurements was  $\pm 1$   $\mu\text{V}$ . The average error in the measurement of resistivity was 10% and it was about 5% in thermoelectric power measurement.

### III. RESULTS AND DISCUSSION

#### A. Structural analysis

##### 1. X-ray diffractometry of $\text{Bi}_{93}\text{Sb}_7$

The x-ray diffraction pattern in Fig. 1 shows that the powders of bulk, as-grown, and annealed  $\text{Bi}_{93}\text{Sb}_7$  thin films are polycrystalline in nature. The indexing of the XRD pattern of the alloy was done in comparison with the American Society for Testing of Materials (ASTM) standard data available for the elements Bi and Sb (Refs. 20 and 21) and the

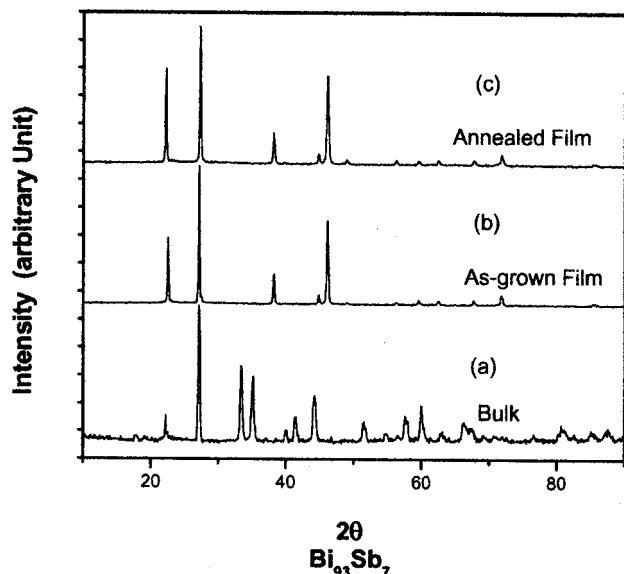


FIG. 1. XRD pattern of (a) bulk  $\text{Bi}_{93}\text{Sb}_7$  alloys, (b) as-grown, and (c) annealed films [intensity (arbitrary unit) vs  $2\theta$ ].

data of Devaux *et al.*<sup>21</sup> The comparison of the alloy  $d$  values with those of bismuth and antimony is shown in Table I. It can be seen that there is a reasonably good agreement of our observed  $d$  values with those of Devaux *et al.*<sup>21</sup> Bismuth and antimony  $d$ -value data of the elements are also given in the table for comparison.

## 2. Transmission electron microscopy (TEM) results

The study of structure and surface morphology was carried out using TEM in both as-grown and annealed films grown on glass substrates. Here Figs. 2(a) and 2(b) show the electron micrograph and the SAED pattern inserted as inset of 100-nm thickness of as-grown and annealed films. It can be seen that there is an increase in grain size after annealing to more than double the as-grown film value due to annealing of the as-grown film. The measured average grain size of the as-grown film is  $\cong 23$  nm and that of the annealed film is

$\cong 55$  nm. From the SAED pattern, we observe that after annealing, there are slightly larger number of diffraction lines, which are due to an increase in the size of the grains and removal of voids or point defect clusters, leading to stronger and detectable diffraction maxima. Missana *et al.*<sup>22,23</sup> have shown that the interdiffusion between Bi and Sb layers occurs and they have reported that there are many voids present in their sample, which may be due to the lattice defect clusters and grain boundaries. We have also observed similar properties in homogeneous alloys of  $\text{Bi}_{88}\text{Sb}_{12}$ ,  $\text{Bi}_{80}\text{Sb}_{20}$ , and  $\text{Bi}_{85}\text{Sb}_{15}$  thin films. After annealing, these voids or lattice defect clusters decrease and there is an increase in grain size. From the thermoelectric application point of view, the polycrystalline material is better than the single-crystalline one and others because the device failure possibility is less.

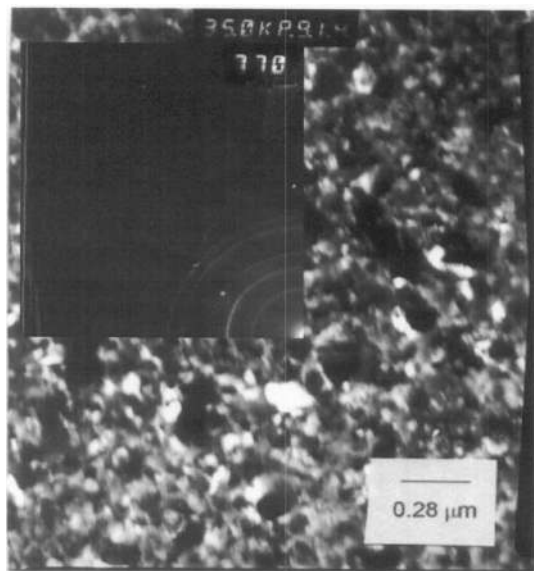
## B. Compositional analysis of $\text{Bi}_{93}\text{Sb}_7$

### 1. Analysis by PIXE

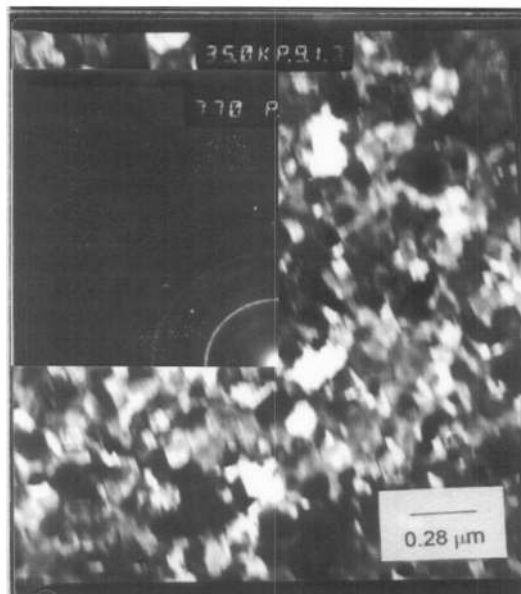
The particle-induced x rays generated corresponding to the constituent elements of the compounds, namely, bismuth and antimony are indicated in the spectra. For both bismuth and antimony characteristic  $L_{\alpha 1}$  x-ray emission lines are seen. There is no interference of x-ray emission lines. This is due to the fact that the elements bismuth and antimony do not lie close in the periodic table, and hence, the difference between their characteristic x-ray energies is greater than the resolution of the detector. The PIXE spectra analysis was performed using the GUPIX software. This simulation program gives a nonlinear least-square fitting of the experimental data along with the subsequent conversion of peak intensities into composition of the elements. The program requires experimental geometry, Si(Li) detector solid angle parameter, and other experimental conditions such as energy of the incident beam, current, and charge. Concentration of bismuth and antimony was estimated from the  $L$  x rays. The results are given in Table II.

TABLE I. XRD and TEM results of bulk  $\text{Bi}_{93}\text{Sb}_7$  as-grown, and annealed thin films.

SL No.	ASTM $d$ values ( $\text{\AA}$ )			ASTM $d$ values ( $\text{\AA}$ )			Observed $d$ values of $\text{Bi}_{93}\text{Sb}_7$ ( $\text{\AA}$ )			
	Bismuth $l$	Bismuth $hkl$	Intensity	Antimony $l$	Antimony $hkl$	Intensity	Ref. 18 XRD $d$ value	Bulk XRD $d$ value	SAED as-grown $d$ value	Thin film SAED annealed $d$ value
1	3.1430	0 0 3	9	2.9862	0 0 3	25	3.97	3.9376		3.924
2	2.975	1 0 1	3	2.8152	[1 0 1]	4	3.245	3.2748	3.226	3.232
3	2.609	0 1 2	100	2.4739	[0 1 2]	100	2.387	2.3528		
4	1.901	1 0 4	40	1.7123	[1 0 4]	70	2.2892	2.2697	2.244	
5	1.808	1 1 0	41	1.5349	1 1 0	56	2.0405	2.0231		
6	1.615	0 1 5	8	1.4943	[0 1 5]	12	1.9703	1.9686		
7	1.572	0 0 6	3	1.4084	0 0 6	35	1.8686	1.8693	1.843	1.843
8	1.567	1 1 3	10	1.2373	[2 0 2]	26	1.6379	1.6350		
9	1.544	0 2 1	1	1.1768	[0 2 4]	13	1.5595	1.5545		
10	1.486	2 0 2	23	1.1434	[1 0 7]	12	1.4863	1.4827		
11	1.304	0 2 4	9	1.1267	[2 0 5]	63	1.4369	1.4353	1.443	1.445
12	1.238	1 0 7	6	1.0885	1 1 6	67		1.3859		
13	1.205	2 0 5	2	1.0487	[1 2 2]	30				
14	1.186	1 1 6	13	1.0034	[0 1 8]	40				



(a)



(b)

FIG. 2. (a) and (b) TEM micrograph of as-grown film with selected area electron diffraction pattern of as-grown and annealed films.

## 2. Analysis by RBS

Figures 3(a) and 3(b) show the typical RBS spectra of  $\text{Bi}_{93}\text{Sb}_7$  as-grown and annealed films grown on the silicon substrate at room temperature. The dotted curve corresponds to the experimental data and the continuous line is the simulated fitting.

TABLE II. The elemental composition and observed value from PIXE and RBS.

Elements	Initial composition	PIXE bulk concentration (%)	RBS as-grown thin-film concentration (%)	RBS annealed thin-film concentration (%)
Bi	93	92.98	92.65	92.65
Sb	7	7.12	07.35	07.35

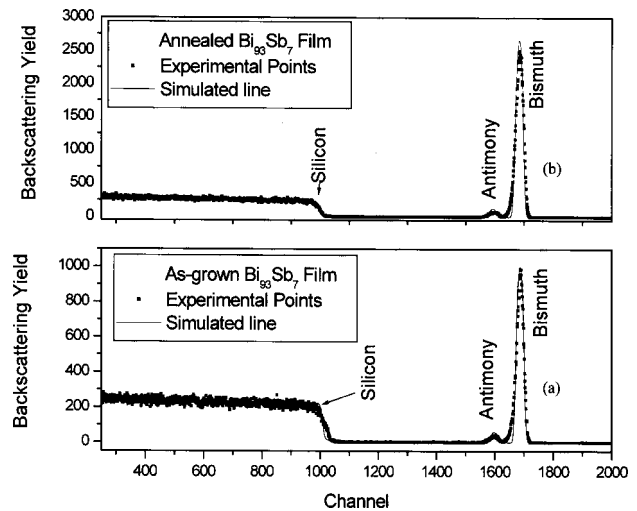


FIG. 3. (Channel number vs yield) backscattering spectra of  $\text{Bi}_{93}\text{Sb}_7$  (a) as-grown and (b) annealed thin films grown onto silicon substrates.

The spectrum consists of two superimposed elemental yields of two atomic species present in  $\text{Bi}_{93}\text{Sb}_7$ . The highest channel number corresponds to the highest backscattered energy of  $\text{He}^{++}$  ion from the heavier element bismuth and lighter antimony present in the compound. The edge occurring at a channel below 950 is due to the silicon substrate. The energy channel corresponding to bismuth is 1685 and antimony is 1587. The annealing effect was observed in RBS too. We have observed that after annealing, the grain size increases and the grains tend to orient in a preferred crystallographic direction. There may be a possibility of channeling and due to this, the RBS spectra can become broader. The result obtained from the RBS experiment is that the composition is intact in thin films too with minor variation and a slight decrease in Bi concentration and an increase in Sb concentration. The thickness measured *in situ* is comparable to the thickness obtained by the RBS simulation within an error of  $\pm 30 \text{ \AA}$  (3 nm). Details of the composition and thickness measurements are given in Table II.

## C. Electrical resistivity data analysis

Figures 4(a) and 4(b) show the electrical resistivity of as-grown and annealed films as a function of the inverse of film thickness at different temperatures. The electrical resistivity measurements were made on as-grown and annealed films in the temperature range of 100–300 K using the van der Pauw method. It is found that the resistivity of as-grown films is more than that of the annealed films. This is because of the annealing effect. On annealing, the defects, especially point defect clusters, will be reduced and also there will be a grain-size increase, thereby reducing the grain-boundary area. Both of these contribute to a decrease in charge-carrier scattering.

## D. Thermoelectric power data analysis

Thermoelectric power measurements on the as-grown as well as annealed films show that the material is *n* type, as the thermoelectric power is negative. Figures 5(a) and 5(b) show the thermoelectric power versus inverse of film thickness

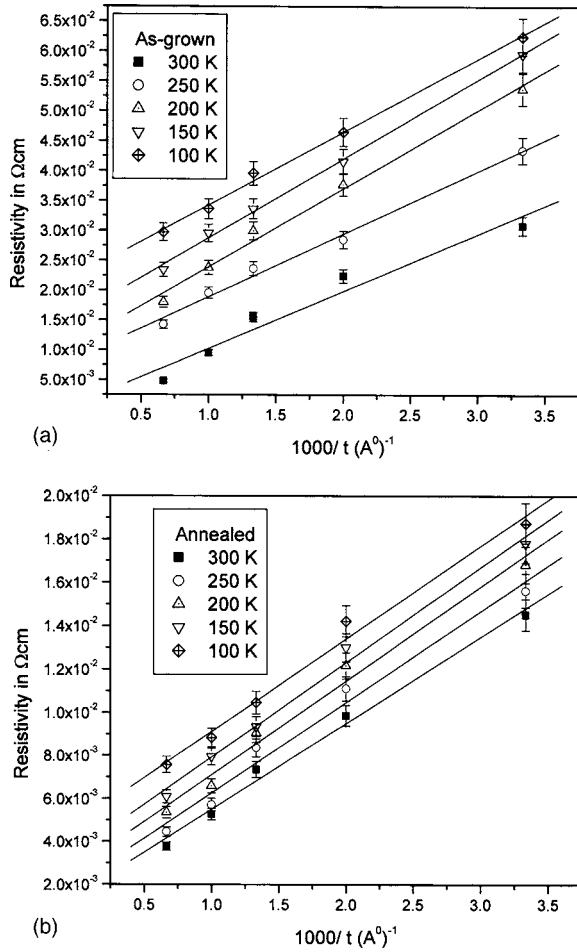


FIG. 4. (a) and (b) Resistivity vs inverse of film thickness for  $(\text{Bi}_{93}\text{Sb}_7)$  as-grown and annealed films.

plots of as-grown and annealed films at different temperatures. As seen in Figs. 5(a) and 5(b), there is an increase in the absolute value of thermoelectric power (which is negative) with an increase in film thickness, as expected. The thermoelectric power increases after annealing the sample also, which can be seen by a careful comparison of thermoelectric power values of Figs. 5(a) and 5(b) for a film of particular thickness at a particular temperature. The above result is anticipated because this increase is due to the increase in the grain size of the films upon annealing. The thermoelectric power of the films was calculated from the measured thermal emf values by the least-squares error analysis using spline functions. It can also be seen that both in as-grown films and annealed films, as the temperature increases the absolute value of thermoelectric power (which is negative) increases.

### E. Calculation of power factor and scattering index parameter from thermoelectric power and resistivity data

To determine the power factor and scattering index parameter, a number of theories<sup>24-26</sup> have been suggested. Teller and co-workers<sup>24,25</sup> have suggested a simple model for electrical resistivity and thermoelectric power as a function of thickness. We are interested to know the nature of scatter-

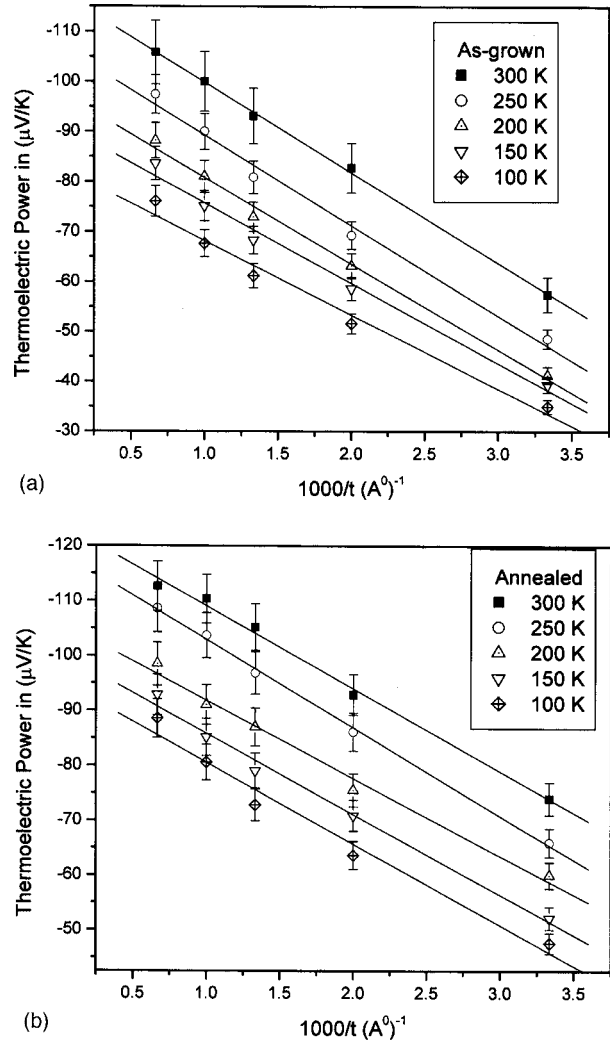


FIG. 5. (a) and (b) Thermoelectric power vs inverse of film thickness for  $(\text{Bi}_{93}\text{Sb}_7)$  as-grown and annealed films.

ing that occurs in  $\text{Bi}_{93}\text{Sb}_7$  thin films which influences the figure of merit  $Z$  which is defined as  $S^2\sigma/K$ , where  $S$  is the thermoelectric power,  $\sigma$  is the electrical conductivity, and  $K$  is the thermal conductivity. The figure of merit  $Z$  depends on the scattering mechanism occurring in the thin films as is described elsewhere.<sup>27</sup>

Now the position of the Fermi level in a material depends on the concentration of charge carriers which in turn depends on the impurities in the material.  $Z$  varies from one material to another material depending on the electron-hole concentration and impurities and defects. The optimum position of the Fermi level is found by setting  $(dz/d\eta)=0$ , so  $Z$  will be taking the form

$$\eta + 4 \left( \frac{5}{2} + \lambda \right) \frac{k^2}{e} \text{FGT} \exp \eta = \frac{1}{2} + \lambda. \quad (1)$$

In semiconducting materials, the lattice component of thermal conductivity is greater than the electronic component. Due to this reason, the second term on the left-hand side of the above equation is negligible. So  $\eta=(1/2+\lambda)$ . The value of  $\lambda$  will give information about the nature of scattering occurring in the thin films.  $\lambda$  value lies between  $-1/2$  and  $3/2$

TABLE III. The physical parameters [hypothetical bulk resistivity ( $\rho_g$ ), Seebeck coefficient ( $S_g$ ), mean free path ( $l_g$ ), energy-dependent term  $U_g$ , and Fermi energy ( $E_F$ )] observed from the analysis of TEP and resistivity data of  $\text{Bi}_{93}\text{Sb}_7$  (a) as-grown films and (b) annealed films.

Temperature (K)	$\rho_g(\Omega \text{ cm})$	$S_g(\mu\text{V/K})$	$l_g(\text{\AA})$	$U_g$	$E_F(\text{meV})$
100	0.022 02	-83.1	3814	$-1.25 \times 10^{-4}$	29.322 67
150	0.0155	-91.8	3566	$-1.38 \times 10^{-4}$	39.820 27
200	0.0108	-97.18	3234	$1.438 \times 10^{-4}$	50.1471
250	0.008 35	-107	2277	$1.978 \times 10^{-4}$	56.747 51
300	$6 \times 10^{-4}$	-117	1480	$2.75 \times 10^{-4}$	62.506 75
Temperature (K)	$\rho_g(\Omega\text{cm})$	$S_g(\mu\text{V/K})$	$l_g(\text{\AA})$	$U_g$	$E_F(\text{meV})$
100	0.0633	-99	6000	$-8.624 \times 10^{-5}$	24.595 86
150	0.061 07	-103	5400	$-9.01 \times 10^{-5}$	35.382 43
200	0.558	-106.5	4200	$-1.047 \times 10^{-4}$	45.985 73
250	0.0484	-122	3300	$-1.362 \times 10^{-4}$	49.944 63
300	0.040 73	-129	2300	$-1.804 \times 10^{-4}$	56.682 14

and thus the value of  $\eta$  should lie between 0 and 2.

In order to determine the value of  $\lambda$ , we have applied the classical size effect theory of thin films. According to the effective mean-free-path model of the classical size effect theory of Tellier and co-workers<sup>24,25</sup> we have for the thermoelectric power  $S_F$  and the electrical resistivity  $\rho_F$  of the films the expressions

$$\rho_F = \rho_g \left[ 1 + \frac{3}{8}(1-P) \frac{l_g}{t} \right], \quad (2)$$

and

$$S_F = S_G \left[ 1 - \frac{3}{8}(1-P) \left( \frac{U_g}{1+U_g} \right) \frac{l_g}{t} \right], \quad (3)$$

where  $S_g$  and  $\rho_g$  are thermoelectric power and electrical resistivity of the infinite thickness film, i.e., the bulk material having the same microstructure as of the thin films being studied,  $t$  is the thickness,  $p$  is the specularity parameter, and  $l_g$  is the mean free path in the filmlike bulk. These equations are valid for films of thicknesses  $t \sim l_g$ ,

$$U_g = (d \ln[l_g]) / (d \ln[E]) \text{ at } E = E_F, \quad (4)$$

where  $E_F$  is the Fermi energy. It is clear from Eqs. (2) and (3) that plots of  $\rho_F$  and  $S_F$  against  $1/t$  will be linear as observed, and the intercepts on the y axis (resistivity or thermoelectric power axis, respectively) will give  $\rho_g$  and  $S_g$ , respectively. From Figs. 5(a) and 5(b) we get the  $S_g$  value of the filmlike bulk material at different temperatures before and after annealing the films. From Figs. 4(a) and 4(b) we get the  $\rho_g$  value of the filmlike bulk material at different temperatures before and after annealing the films. From the slopes of the different straight-line plots (at different temperatures) of Fig. 4(a) and 4(b), we have calculated the  $l_g$  values, as the slope is equal to  $\frac{3}{8}(1-P)(l_g)(\rho_g)$ . We have also calculated the  $U_g$  values from the slopes of straight-line plots of Figs. 5(a) and 5(b) at different temperatures by equating the slope to  $\frac{3}{8}(1-P)(U_g/(1+U_g))(S_G)(l_g)$ .

Tables III(a) and III(b) show the various parameters calculated from the experimental data. It can be seen from both plots in Figs. 4(a), 4(b), 5(a), and 5(b) and Tables III(a) and

III(b) that as the film thickness increases, the resistivity decreases (for a particular temperature) and as the temperature increases also resistivity decreases (for a particular film thickness). The calculated mean-free-path value decreases with an increase in temperature both for as-grown and annealed films, as is expected.

Jain and Verma<sup>28,29</sup> have developed a size effect theory considering that the relaxation time is not a constant but a function of energy of the carriers. They assumed that the relaxation time  $\tau$  varies as some power  $\lambda$  of the energy of the carriers  $E$  and wrote the relaxation time  $\tau$  as a function of the energy of the carriers,  $E$  as  $\tau = aE^\lambda$ , where  $a$  and  $\lambda$  are constants. The value of the index parameter  $\lambda$  depends upon the scattering processes predominant in the films, as the energy dependences of the relaxation time will be different for different scattering processes. They obtained expressions for the size dependence of electrical conductivity  $\sigma_F$  and thermoelectric power  $S_F$  as expressions in terms of reduced thickness  $K_g$  and scattering parameter which are given elsewhere<sup>28,29</sup> where  $K_g = t/l_g$  is the thickness measured in the units of the mean free path  $l_g$  and  $p$  is the specularity parameter giving the fraction of the carriers that are scattered specularly from the surfaces, and takes values between 1 and 0.  $\lambda$  is the energy power index defined earlier.  $\theta$  is the angular position variable.

If we assume that all the carriers are diffusely scattered from the film surfaces, then we have  $p=0$ . Then, the equations for thermoelectric power  $S_F$  and conductivity  $\sigma_F$  reduce to

$$\frac{S_F}{S_g} = 1 - \frac{(\lambda + 1/2)K_g}{(\lambda + 3/2)} \left( \frac{\partial F}{\partial K_g} \right) p = 0, \quad (5)$$

$$\frac{\sigma_F}{\sigma_g} = 1 - \frac{(\lambda + 1/2)K_g}{(\lambda + 3/2)} \left( \frac{\partial F}{\partial K_g} \right) p = 0. \quad (6)$$

Thus, it is seen that the variation of the thermoelectric power ratio ( $S_F/S_g$ ) with the reduced thickness  $K=t/l_g$  is a function of  $\lambda$ , the scattering parameter. Using the above equation, plots of  $S_F/S_g$  against  $t/l_g$  can be drawn for different values of the scattering index  $\lambda$ . Using the value of  $l_g$ , the ratio

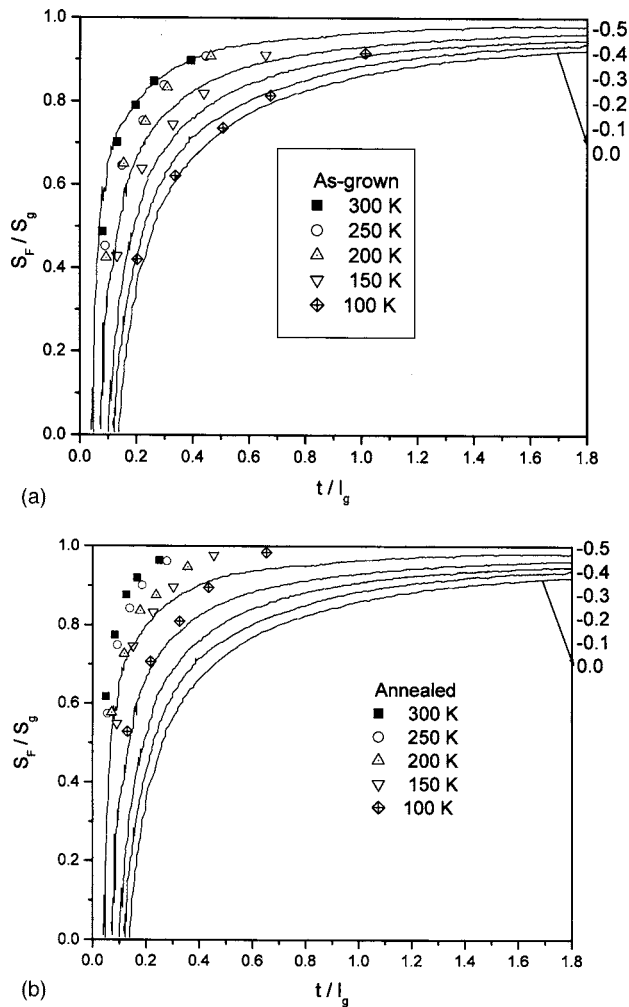


FIG. 6. (a) and (b) Thermoelectric power of thin films ( $S_F$ ) / thermoelectric power of bulk material ( $S_g$ ) vs thickness ( $t$ )/mean-free-path ( $l_g$ ) theoretical plots and data points for ( $\text{Bi}_{93}\text{Sb}_7$ ) as-grown and annealed thin films.

$K=t/l_g$  can be determined, and hence, experimental data points of  $S_F/S_g$  against  $t/l_g$  can be plotted and compared with the plots according to the above equation. Hence, the value of the scattering index parameter  $\lambda$  can be evaluated.

Figures 6(a) and 6(b) show the plots of  $S_F/S_g$  against  $t/l_g$  for different temperatures. The  $\lambda$  value lies between  $-0.4$  and  $-0.1$  for as-grown films and  $-0.5$  and  $-0.4$  mostly for annealed films for all other temperatures except for the data at 100 K for which they lie close to  $\lambda=-0.3$ . Thus, from this analysis it is found that the scattering is not purely lattice scattering as for lattice scattering  $\lambda$  value will be  $-0.5$ . It is also seen from Figs. 6(a) and 6(b) that upon annealing the films, because most of the defects are annealed out, the scattering approaches predominantly lattice scattering, as the data points crowd around between the curves for  $\lambda=-0.5$  and  $-0.4$  at higher temperatures (except at 100 K where they are close to  $\lambda=-0.3$ ). The  $\lambda$  value at 100 K of  $-0.3$  indicates that there is more of impurity or defect scattering at the lower temperature of 100 K compared to that at higher temperatures. This is understandable as, at low temperatures defect or impurity scatterings become pronounced.

The thermoelectric power factor  $S^2\sigma$  was calculated at different temperatures from the measured thermoelectric

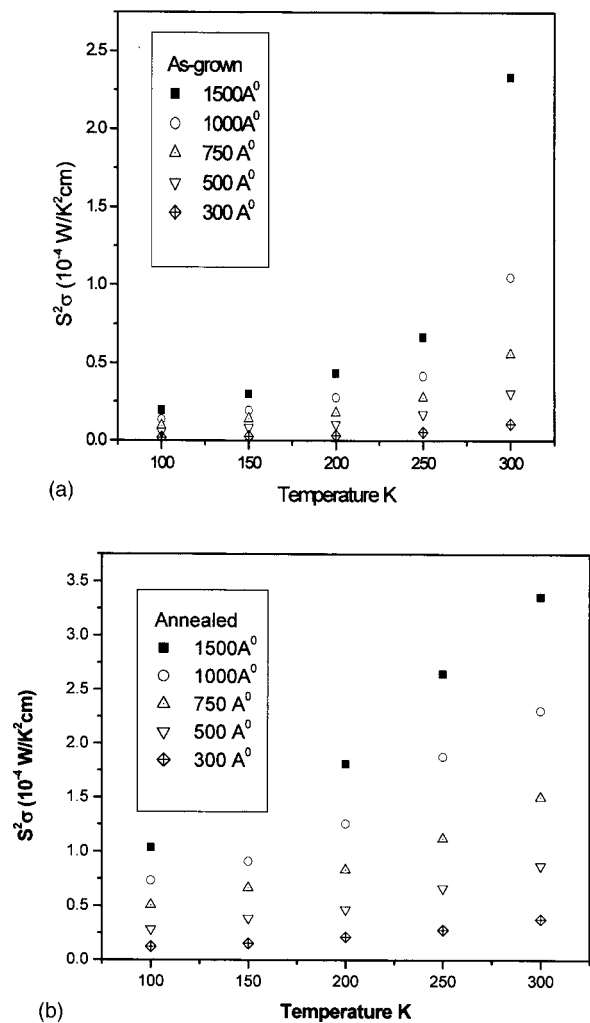


FIG. 7. (a) and (b) Temperature vs thermoelectric power factor of ( $\text{Bi}_{93}\text{Sb}_7$ ) as-grown and annealed thin films.

power and electrical conductivity values. The plots of  $S^2\sigma$  versus temperature for different film thicknesses are shown in Figs. 7(a) and 7(b). It is seen from the figures that the thermoelectric power factor is a function of film thickness and temperature and is also influenced by annealing. It increases both as the film thickness increases and as the temperature increases. Also, annealing of the films causes an increase in the power factor of a film of given thickness at a given temperature.

These values obtained by us for  $\text{Bi}_{93}\text{Sb}_7$  alloy thin films have been compared with the previous reported values for  $\text{Bi-Se-Te}$  and  $\text{Bi}_2\text{Te}_3$  materials. For example, at 300 K, for a film of 1250-Å thickness, our  $S^2\sigma$  values are  $2.5 \times 10^{-4} \text{ W/K}^2 \text{ cm}$  before annealing and  $3.5 \times 10^{-4} \text{ W/K}^2 \text{ cm}$  after annealing. After annealing the value was only  $0.8 \times 10^{-6} \text{ W/K}^2 \text{ cm}$  for  $\text{Bi-Se-Te}$  films,<sup>30,31</sup> which is two orders of magnitude less. When compared to the results of  $\text{Bi}_2\text{Te}_3$  of Zou *et al.*<sup>32</sup> too, our  $\text{Bi}_{93}\text{Sb}_7$  alloy values are also better than those obtained in their work, but are only higher by about one order (their maximum values of  $1.8 \times 10^{-5}$  and  $4.0 \times 10^{-5} \text{ W/K}^2 \text{ cm}$  for  $p$ - and  $n$ -type  $\text{Bi}_2\text{Te}_3$ , respectively). Thus, our power factor values are more than 100 times larger in comparison with those of Refs.

30 and 31, and are about 10 times larger than those of Zou *et al.*<sup>32</sup> When we compare our power factor values of Bi<sub>93</sub>Sb<sub>7</sub> alloy films with the value calculated using the data on bulk Bi<sub>92.9</sub>Sb<sub>7.1</sub> alloy obtained by Lenoir *et al.*,<sup>3</sup> which is around  $8 \times 10^{-4}$  W/K<sup>2</sup> cm, it is found that our power factor values are of the same order as those of the bulk values, but are smaller by a factor of about 3–4.

#### IV. CONCLUSIONS

The flash evaporation technique was used to prepare the thin films of Bi<sub>93</sub>Sb<sub>7</sub> alloys. The prepared thin films maintain the stoichiometry, which was verified by the RBS experiments. The XRD and TEM results show that the bulk and the thin films are of the same phase. Both the prepared bulk alloy and thin films show polycrystalline nature. The grain size of the films increases with annealing of the films. The thickness dependence of thermoelectric power and electrical resistivity is explained by the classical size effect theory. Thermoelectric power factor of annealed films is more than that of the as-grown films due to the increase in grain size and decrease in scattering. The measured negative thermoelectric power for all film thicknesses indicates *n*-type conductivity (majority electron conductivity) of the films. The thickness dependence of thermoelectric power and electrical resistivity is explained using the classical size effect theory based on the model of Tellier and co-workers. Various physical parameters have been calculated using this model. Mean free path increases with the increase of temperature, as is expected. The negative value of the parameter  $U_g$  indicates that the electron-phonon interaction is the main scattering mechanism in the material. The Fermi energy value varies slightly with temperature. The scattering index parameter was calculated in both as-grown and annealed films. Both the electrical conductivity and thermoelectric power of annealed films are larger than those of as-grown films.

#### ACKNOWLEDGMENTS

One of the authors, (R.C.M.) would like to thank IIT Madras, for providing financial assistance for carrying out the research. We would like to thank Institute of Physics, Bhubaneswar, Orissa, India for providing the RBS facility and Kanchanamala of Metallurgy Department, IIT, Madras for the TEM study. One of the authors (V.D.D.) thanks the

Alexander von Humboldt Foundation for a reinvention fellowship during his stay in Germany during this work.

- <sup>1</sup>N. B. Mustafaev, *J. Phys.: Condens. Matter* **6**, 2039 (1994).
- <sup>2</sup>J. M. Ziman, *Electrons and Phonons The Theory of Transport Phenomena in Solids* (Oxford University Press, London, 1960), p. 123.
- <sup>3</sup>B. Lenoir, M. Cassart, J. P. Michenaud, H. Scherrer, and S. Scherrer, *J. Phys. Chem. Solids* **57**, 89 (1996).
- <sup>4</sup>A. L. Jain, *Phys. Rev.* **114**, 1518 (1959).
- <sup>5</sup>S. Cho, A. DiVenere, G. K. Wong, J. B. Ketterson, and J. R. Meyer, *J. Appl. Phys.* **85**, 3655 (1999).
- <sup>6</sup>S. Cho Y. Kim, S. J. Youn, A. DiVenere, G. K. Wong, A. J. Freeman, and J. B. Ketterson, *Phys. Rev. B* **64**, 235330 (2001).
- <sup>7</sup>P. M. Hansen, *Constitution of Binary Alloys* (McGraw-Hill, New York, 1958), p. 332.
- <sup>8</sup>A. Armigliato, G. G. Bentini, S. Guerri, P. Ostojica, and L. Morettini, *Thin Solid Films* **33**, 353 (1976).
- <sup>9</sup>G. Linker, O. Meyer, and M. Gettings, *Thin Solid Films* **19**, 177 (1973).
- <sup>10</sup>T. G. Finstad, T. Andreassen, and T. Olsen, *Thin Solid Films* **29**, 145 (1975).
- <sup>11</sup>D. V. Morgan, *J. Phys. D* **7**, 653 (1974).
- <sup>12</sup>J. A. Moore, I. V. Mitchell, M. J. Hollis, J. A. Davies, and M. Howe, *J. Appl. Phys.* **46**, 52 (1975).
- <sup>13</sup>K. Sekar, P. V. Satyam, G. Kuri, D. P. Mahapatra, and B. N. Dev, *Nucl. Instrum. Methods Phys. Res. B* **73**, 63 (1993).
- <sup>14</sup>K. Sekar, G. Kuri, P. V. Satyam, B. Sundaravel, D. P. Mahapatra, and B. N. Dev, *Indian J. Phys., A* **68A**, 1 (1994).
- <sup>15</sup>R. Rout, S. K. Ghose, D. P. Mahapatra, B. N. Dev, H. Bakhru, and A. W. Haberl, *Nucl. Instrum. Methods Phys. Res. B* **181**, 110 (2001).
- <sup>16</sup>J. L. den Besten, L. J. Allen, and D. N. Jamieson, *Phys. Rev. B* **60**, 3120 (1999).
- <sup>17</sup>J. P. Stoquert and T. Szorenyi, *Phys. Rev. B* **66**, 144108 (2002).
- <sup>18</sup>G. Falcon, L. Forlano, and A. I. Tolmachev, *Phys. Rev. B* **60**, 6352 (1999).
- <sup>19</sup>W. R. Runyan, *Semiconductor Measurements and Instrumentation* (McGraw-Hill, New York, 1975), p. 65.
- <sup>20</sup>R. Martin-Lopez, B. Lenoir, X. Devaux, A. Dauscher, and H. Scherrer, *Mater. Sci. Eng., A* **248**, 147 (1998).
- <sup>21</sup>X. Devaux, F. Brochin, A. Dauscher, B. Lenoir, R. Martin-Lopez, H. Scherrer, and S. Scherrer, *Nanostruct. Mater.* **8**, 137 (1997).
- <sup>22</sup>T. Missana, C. N. Afonso, A. K. Petford-Long, and C. R. Doole, *J. Magn. Mater.* **156**, 281 (1996).
- <sup>23</sup>T. Missana, C. N. Afonso, A. K. Petford-Long, and C. R. Doole, *Thin Solid Films* **288**, 186 (1996).
- <sup>24</sup>C. R. Pichard, C. R. Tellier, and A. J. Tosser, *J. Phys. F: Met. Phys.* **10**, 2009 (1980).
- <sup>25</sup>C. R. Tellier, *Thin Solid Films* **51**, 311 (1978).
- <sup>26</sup>C. R. Tellier and A. J. Tosser, *Thin Solid Films* **41**, 161 (1977).
- <sup>27</sup>H. J. Goldsmid, *Application of Thermoelectricity* (Wiley, New York, 1960), p. 41.
- <sup>28</sup>G. C. Jain and B. S. Verma, *Thin Solid Films* **15**, 191 (1973).
- <sup>29</sup>G. C. Jain and B. S. Verma, *Thin Solid Films* **11**, 389 (1972).
- <sup>30</sup>V. Damodara Das and S. Selvaraj, *J. Appl. Phys.* **83**, 3696 (1998).
- <sup>31</sup>V. Damodara Das and S. Selvaraj, *J. Appl. Phys.* **86**, 1518 (1999).
- <sup>32</sup>H. Zou, D. M. Rowe, and G. Min, *J. Cryst. Growth* **222**, 82 (2001).